RSC Advances

PAPER

View Article Online
View Journal | View Issue

Cite this: *RSC Adv.*, 2018, **8**, 13493

Preparation of a balsa-lysozyme eco-friendly dressing and its effect on wound healing

Daijun Zhou, Tao Yang, Malcolm Xing* and Gaoxing Luo*

Received 26th March 2018
Accepted 27th March 2018

DOI: 10.1039/c8ra02629g

rsc.li/rsc-advances

This study aims to prepare an eco-friendly dressing using a balsa derived membrane with lysozyme included for anti-bacterial purposes. The balsa-lysozyme was prepared using delignification (control) and dopamine (group A) methods for mussel-inspired adhesion of 5, 10, 15 and 20 mg ml^{-1} lysozyme (groups B, C, D and E). Fourier infrared spectra and the contact angle test showed that lysozyme adhered to the membrane. With increasing concentration of lysozyme, the drug-loading rate of balsa-lysozyme increased and the encapsulation efficiency decreased ($P < 0.05$). The cumulative release percentages after 72 h were 80.7%, 90.6%, 91.4%and 92.3% in groups B, C, D and E, respectively. There was a significant *in vitro* antibacterial effect against both *E. coli* and *S. aureus*. The cytotoxicity of the wood dressing was not detected until day 7. On day 7, the healing rates were 30.7%, 38.3%, 50.7%, 61.2%, 61.9% and 62.4% for the control, A, B, C, D and E group ($P < 0.05$). Similarly, the lengths of the new epithelium were 631.7 μm, 702.5 μm, 759.4 μm, 825.3 μm, 831.7 μm and 836.6 μm for the control group, A, B, C, and D, E respectively ($P < 0.05$). Furthermore, PCNA and CD31 expression indicated enhanced cell proliferation and angiogenesis in the C, D and E group ($P < 0.05$).

1 Introduction

Wood is the most widely used biological building material. Although its origin from renewable resources (trees) is attractive, its widespread use is mainly due to building tradition, competitive cost, and good material properties.[1] These include low density, high modulus, high strength, high toughness, and low thermal conductivity. Recent research shows interesting possibilities to modify wood templates in order to add functional properties. Furthermore, this polymeric nanocomposite is synthesized at ambient temperature and pressure, by the plant itself, using carbon dioxide and water.[2,3] Balsa wood is soft and light, and has material uniformity, low thermal conductivity, and volume stability.[4] Balsa can be used in a variety of special structures. For example, delignification by polymerization of formaldehyde methyl acrylate can increase light-balsa transmittance by 85%, thereby reducing the balsa thickness and fiber volume fraction, resulting in a modified material with good structural mechanical properties and optical translucency appearance.[5] When applied as a wound dressing substrate, this material may offer low cost and good air permeability (the pore size of wood fiber can reach several microns).

Lysozyme is a small monomer protein of 129 amino acid residues, with anti-inflammatory, anti-virus, bactericidal, and antihistamine activities.[6,7] It has been widely used as an antibacterial agent.[8] Lysozyme degrades peptidoglycan in the bacterial cell wall, leading to rapid killing of Gram-positive organisms. However, lysozyme is inactive against most Gram-negative bacteria because it cannot penetrate the outer membrane to reach its target, the peptidoglycan layer.[9] An additional limitation of lysozyme is that its molecular structure is unstable and easily inactivated. Clinically, it is often used in the form of a microballoon or in combination with other antimicrobial agents.[10,11]

For patients with severe skin defects, there is an urgent need to quickly and effectively close the wound. Effective and inexpensive strategies to prevent bacterial invasion and the loss of body fluids are needed. The combination of lysozyme and wound dressing may allow continuous sterilization effects against Gram-negative bacilli.[12,13] Wound dressings are used to rebuild the skin barrier, accelerate healing, and prepare for later surgery.[14] Ideal wound dressings should have good mechanical properties, proper water vapor permeability, and good biocompatibility. Infection and inflammation will inhibit or prevent wound healing, so the ideal wound dressing should provide a local surface suitable for antibacterial effect.[15,16] Natural materials such as chitin and chitosan, dextran, cellulose, alginate, and silk protein, are considered good wound dressings materials because of their biocompatibility. There is growing interest in the use of natural materials loaded with antibacterial agents, growth factors, or other chemicals, to promote the healing of infectious wounds.[17–19]

The goal of this study was to combine delignified balsa and lysozyme to design a new economic and efficient antimicrobial

Institute of Burn Research, State Key Laboratory of Trauma, Burn and Combined Injury, Key Laboratory of Proteomics of Chongqing, Southwest Hospital, Army Medical University (Third Military Medical University), 30 Gaotanyan Main Street, Shapingba District, Chongqing 400038, China. E-mail: logxw@yahoo.com; malcolm.xing@umanitoba.ca; Fax: +86-023-68975399; Tel: +86-023-68975399

dressing. We then assessed its antibacterial activity *in vitro*, as well as its cytotoxicity and its effect on wound healing.

2 Materials and methods

2.1 Materials

Dopamine hydrochloride and lysozyme were purchased from Solarbio Science & Technology Co., Ltd. (Beijing, China). Balsa was purchased from Lego. BALB/c mice (males, 20–25 g) were obtained from the Experimental Animal Department of the Third Military Medical University. Animals were raised in a room at 25 °C, with a relative humidity of 50%, and a 12 h circadian rhythm. Before the experiment, the mice were fed in single cage and adapted to one week in advance. An overview of the methods is illustrated in the schematic in Fig. 1.

2.2 Animal care ethical statement

In this study, all animal protocols were permitted by the Institutional Animal Care and Use Committee of the Third Military Medical University (TMMU), Chongqing, China. All animal experiments followed the regulation on the management of laboratory animals which was issued by the Chinese Association for Laboratory Animal Sciences (CALAS).

2.3 Delignification

Balsa samples with density of about 160 kg m^{-3} were punched to produce discs (diameter 0.6 cm and thickness 0.8 mm). The discs were dried at 105 ± 3 °C for 24 hours and then immersed in 1% $NaClO_2$-acetate buffer (pH 6.4, 80 °C) for 12 h. The samples were carefully washed with deionized water and then washed three times. Dehydration was performed by ten minute treatments with ethanol, ethanol : acetone, and acetone (1 : 1 : 1). Finally, the wet wood was placed between two pieces of glass and wrapped with aluminum-foil paper. The wet wood was heated in the oven for 4 h at 70 °C for completing the whole polymerization process.

2.4 Dopamine glue with lysozyme

Tris hydrochloric acid (131.14 mg) was dissolved in 100 ml of deionized water, and then 200 mg of dopamine powder was added to prepare a Tris-dopamine solution (2 mg ml^{-1}, pH 8.5). The balsa was then immersed in the dopamine solution for 12 h, and then placed in a shaker at 37 °C (100 rpm). Lysozyme powder was dissolved in deionized water and generated as a 20 mg ml^{-1} lysozyme solution, and then diluted to 0, 5, 10, 15 and 20 mg ml^{-1}, corresponding to the A, B, C, D and E groups. The samples were carefully washed with deionized water, and then incubated in different concentrations of lysozyme solution for 12 h on a 37 °C shaker (100 rpm).

2.5 Scanning electron microscopy (SEM)

The sample of the material wafer was carefully washed with deionized water, dried and sprayed, and the aperture structure of the film was observed under vacuum condition by scanning electron microscope and photographed.

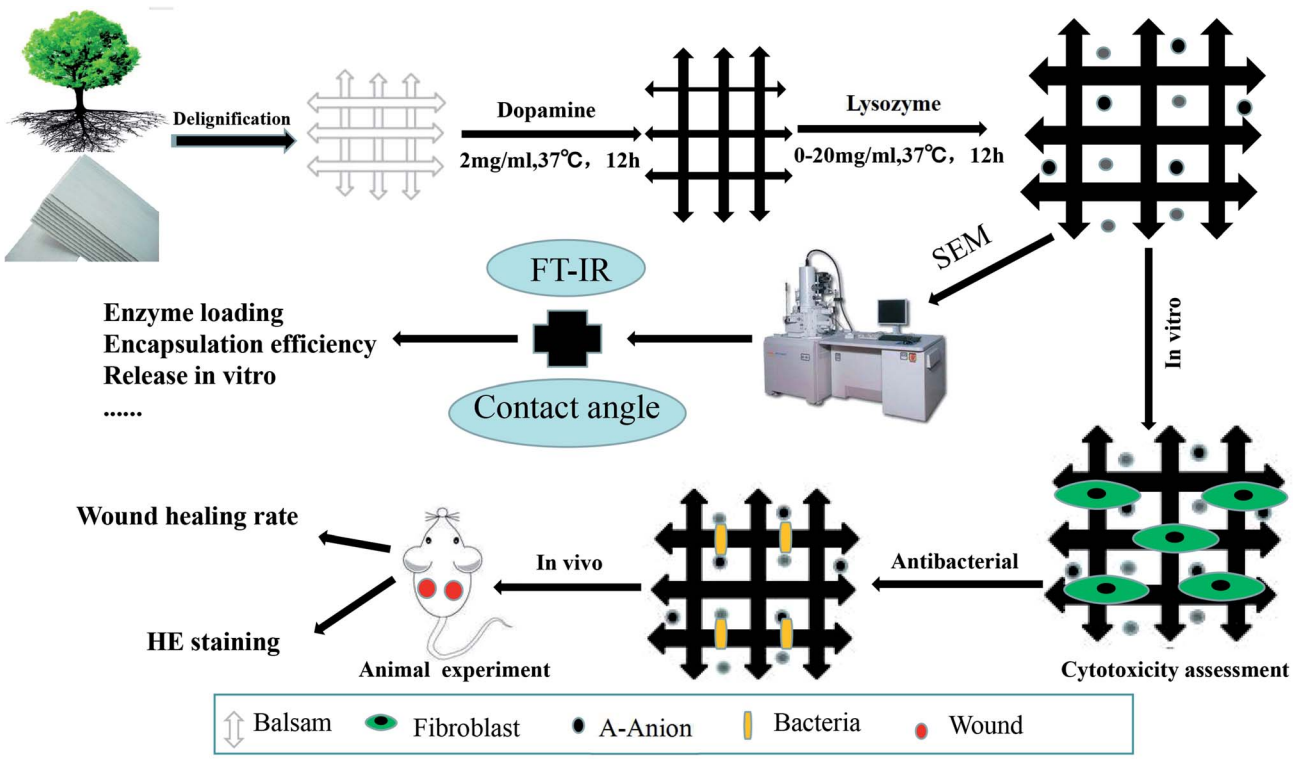

Fig. 1 Schematic illustration of the preparation and evaluation of wood dressing.

2.6 Fourier infrared spectrum

The chemical structures of the different materials were characterized by Fourier transform infrared spectroscopy (Nicolet-460 Thermo Fisher) at a wavenumber scan range of 600–4000 cm^{-1}.

2.7 Contact angle test

The film of different materials was placed on the horizontal surface, and then 1 μl deionized water was dripped down onto the surface of the material. The contact angle size of the droplet was measured, and the average value of each sample was determined from three measurements.

2.8 Drug loading and encapsulation efficiency

2.8.1 Determination of lysozyme standard curve. First, 200 mg of lysozyme was weighed and dissolved in 10 ml phosphate-buffered saline (PBS) at 20 mg ml^{-1}. This solution was diluted with PBS to concentrations of 10 and 5 mg ml^{-1}. The absorbance of the lysozyme solutions at different concentrations was determined at 357 nm by ultraviolet spectrophotometer. The lysozyme concentration as used as the abscissa, and the absorbance was the ordinate to draw a lysozyme standard curve, and the linear regression equation was solved.

2.8.2 Determination of drug loading and encapsulation efficiency. Different concentrations of light wood lysozyme group (BCDE 4 group), 200 mg, liquid nitrogen, frozen powder, and then use ultrasonic dispersion to 10 ml PBS buffer, time 60 min. After removal of the supernatant after centrifugation, the absorbance of the lysozyme solution was determined at 357 nm by ultraviolet spectrophotometer. The standard curve was used to calculate the concentration of lysozyme, and thus calculate the entrapment efficiency and drug loading.

$$\text{Drug loading} = \text{actual lysozyme concentration} \times \text{volume (μg)} / \text{dissolved light wood lysozyme total mass (mg)};$$

$$\text{Encapsulation efficiency} = \text{actual lysozyme concentration} / \text{theoretical lysozyme concentration}$$

2.9 Drug release *in vitro*

Samples of the light wood lysozyme group (BCDE 4 group) were weighed and added to 10 ml PBS buffer, and then placed in a constant temperature shaking table for culturing (37 °C, 70 rpm). At specific time points (0.5 h, 12 h, 24 h, 48 h, and 72 h), the tubes were removed and 2 ml samples of the upper release liquid was removed with a pipette and the absorbance was measured by UV spectrophotometer. When a sample was removed, 2 ml of fresh PBS solution was added to the test tube to maintain the same total volume of the system. Fresh PBS buffer solution was used as the blank control.

According to the lysozyme standard curve, the measured concentration was calculated, and the release amount of light wood lysozyme in each period was calculated. Finally, the cumulative release amount was calculated.

2.10 Bacteria co-culture

Staphylococcus aureus and *Escherichia coli* were obtained from clinical isolate, the Third Military Medical University Southwest Hospital Institute of Burns. First, the bacteria were amplified (grown overnight) to 1×10^9 CFU ml^{-1}, and then diluted with LB medium to 1×10^4 CFU ml^{-1}. The OD value (standard OD = 0.7) of 100 ml bacterial fluid was detected by microplate reader. Each sample was placed into 3 wells (200 μl per well). After incubation at 37 °C for 24 h, the change of OD values was detected. The operations were repeated three times.

2.11 Assay of cytotoxicity

Normal neonatal mice were used to isolate primary fibroblasts according to routine methods and the third passage cells were used to assay the cytotoxicity of the prepared wood-lysozyme dressing. After cells were attached, materials were placed into wells. Each group contained 12 wells (for day 1, 3, 5, and 7 cell proliferation assessment, in triplicate). Each well contained a total volume of 150 μl and the cells were cultured in a 37 °C incubator.

2.12 Mice full-thickness skin defect wound model

Balb/c mice (males, weight 25 g, 8 weeks after birth, normal skin growth) were purchased from the Animal Research Institute of Third Military Medical University. A total of 25 mice were divided equally into five groups according to a random number table. There was no significant difference between the 6 groups in sex, weight, age, or skin growth ($P < 0.05$). The animals were raised for 1 week individually before the experiments, with free access to water and autoclaved rodent chow under standardized conditions (*i.e.*, relative humidity: 50%; circadian rhythm: 12 h; room temperature: 25 °C). One day before the experiment, 1% pentobarbital sodium was injected intraperitoneally (70 μl g^{-1}) and then subjected to depilation. The next day, after the mice were anaesthetized again and disinfected on the back, two skin defect wounds were generated on the left and right sides of the back with a hole punch, for a diameter of 0.6 cm. *S. aureus* and *E. coli* were co-cultured, and 5 μl of the co-culture were added to each wound. The bacterial concentration was 10^8 per ml. Clean materials (disinfected with 75% alcohol, and rinsed with PBS buffer to completely remove the alcohol) were fixed on the wound with an adhesive towel. After 0, 1, 3, 5, and 7 days, photos of the wound were captured and the materials were refreshed.

2.13 Wound healing rate assessment

The wound-healing rate was calculated as follows. IPP6.0 (Image Pro Plus 6.0) software was used to carefully trace the margins of each wound, and calculate the number of pixels encompassed by each wound tracing. The number of pixels was then converted into square millimeters. The extent of wound healing was calculated using the following formula:

$$W = (I - A_n)/I \times 100\%$$

where W represents the percentage of wound healing, I represents the initial wound area, and A_n represents the unhealed wound area on the n^{th} day post-wounding.

2.14 HE staining

At 3 and 7 days post injury, samples of the wound tissue were removed, and paraffin sections were prepared. HE staining was performed according to standard methods. The neonatal epithelial lengths of the samples were measured by different pathologists.

2.15 Western blot to detect PCNA and CD31 expression

To quantitatively assess cell proliferation and angiogenesis in the wound tissues of the different groups, the expression levels of two markers, PCNA and CD31, were determined by western blot on day 5 post-wounding. In brief, full-thickness wound tissues approximately 10 mm × 10 mm in size, including newly regenerated epidermis and granulation tissue, were harvested and immediately transferred to liquid nitrogen. After these samples were ground, lysis buffer (KeyGen, China) was added. The samples were then rotated for 15 min at 4 °C, and then the homogenates were centrifuged at 14 000 rpm for 15 min and the supernatants were collected. Protein concentrations were determined *via* the bicinchoninic acid method in accordance with the instructions for the Varioskan Flash (Thermal Scientific, USA). Equal amounts of protein were boiled for 5 minutes before being loading onto 8% SDS-PAGE gels. Protein samples of 50 mg were used for the western blot analysis. Electrophoresis was performed at 80 volts for 30 min and then at 100 volts for 90 min. The proteins were then transferred to PVDF membranes at 100 volts for 90 min. The PVDF membranes were blocked with tris-buffered saline (TBS) containing 5% bovine serum albumin (Biosharp, China) for 3 hours at 25 °C, and the membranes were then incubated with anti-PCNA antibody (ab15497, Abcam, UK) at a 1 : 1000 dilution, anti-CD31 antibody (ab28364, Abcam, UK) at a 1 : 1000 dilution, or anti-tubulin antibody (Sungene, China) at a 1 : 2000 dilution at 4 °C overnight. The membranes were subsequently washed with TBS containing 1% Tween-20 (TBST) 5 times and then incubated with HRP-labeled goat anti-rabbit secondary antibody (Zhongshan Biology Company, China) at a 1 : 2000 dilution for 1 h at 25 °C. The PDVF membranes were washed with TBST five times and then visualized using chemiluminescence (Thermal Scientific, USA).

2.16 Statistical analysis

All data are presented as the mean ± standard deviation (SD). *T*-tests and one-way ANOVA were used to evaluate statistical significance, followed by post-hoc least significant difference tests. Values of $p < 0.05$ were considered significant.

3 Results

3.1 Electron microscopy scanning

As shown in Fig. 2, the balsa retained ordinary balsa structure under low magnification (Control 1). At medium magnification (Control 2), chemical residues were observed, and at higher magnification (Control 3), the balsa texture was clear and complete. The wood-lysozyme group showed some deposition under E1, E2, and E3. The dopamine layer and lysozyme (as crystals precipitated on the surface) were visible.

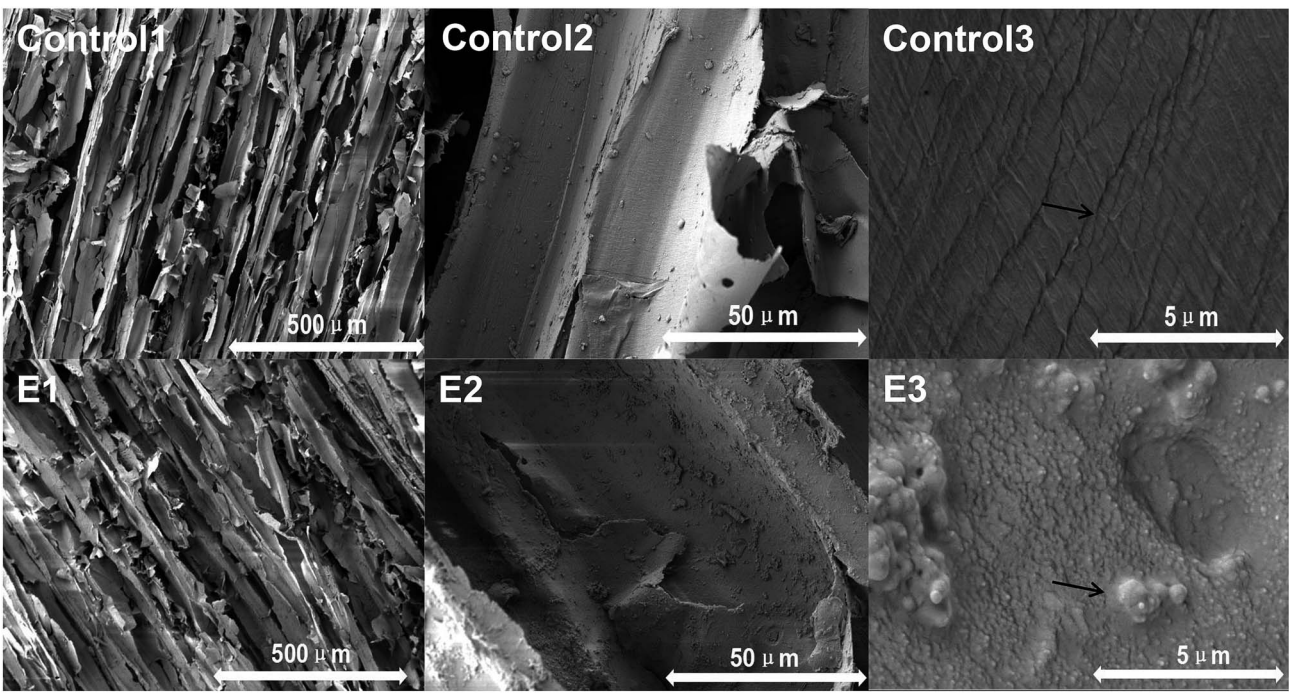

Fig. 2 Representative SEM images of group Control and E. (Control 1–3) delignified balsa. (E1–E3) 20 mg ml^{-1} lysozyme. The black arrows were significantly different in structure, the length of the arrow represents the ruler.

3.2 Fourier infrared spectrum

As shown in Fig. 3, the infrared spectra of three groups were determined (Control, A, and E) and were approximately similar. Peaks of 3328.54 cm^{-1}, 2932.99 cm^{-1}, and 3276.65 cm^{-1} correspond to O–H stretching vibration peaks of hydroxyl groups in balsa fibers. The absorption peak at 1736.90 cm^{-1} and 1736.31 cm^{-1} for the untreated balsa fiber corresponds to the stretching vibration of C–O–C in C–O. The control group region of 1103.99–1364.01 cm^{-1} exhibited broad and strong peaks, which are caused by intermolecular

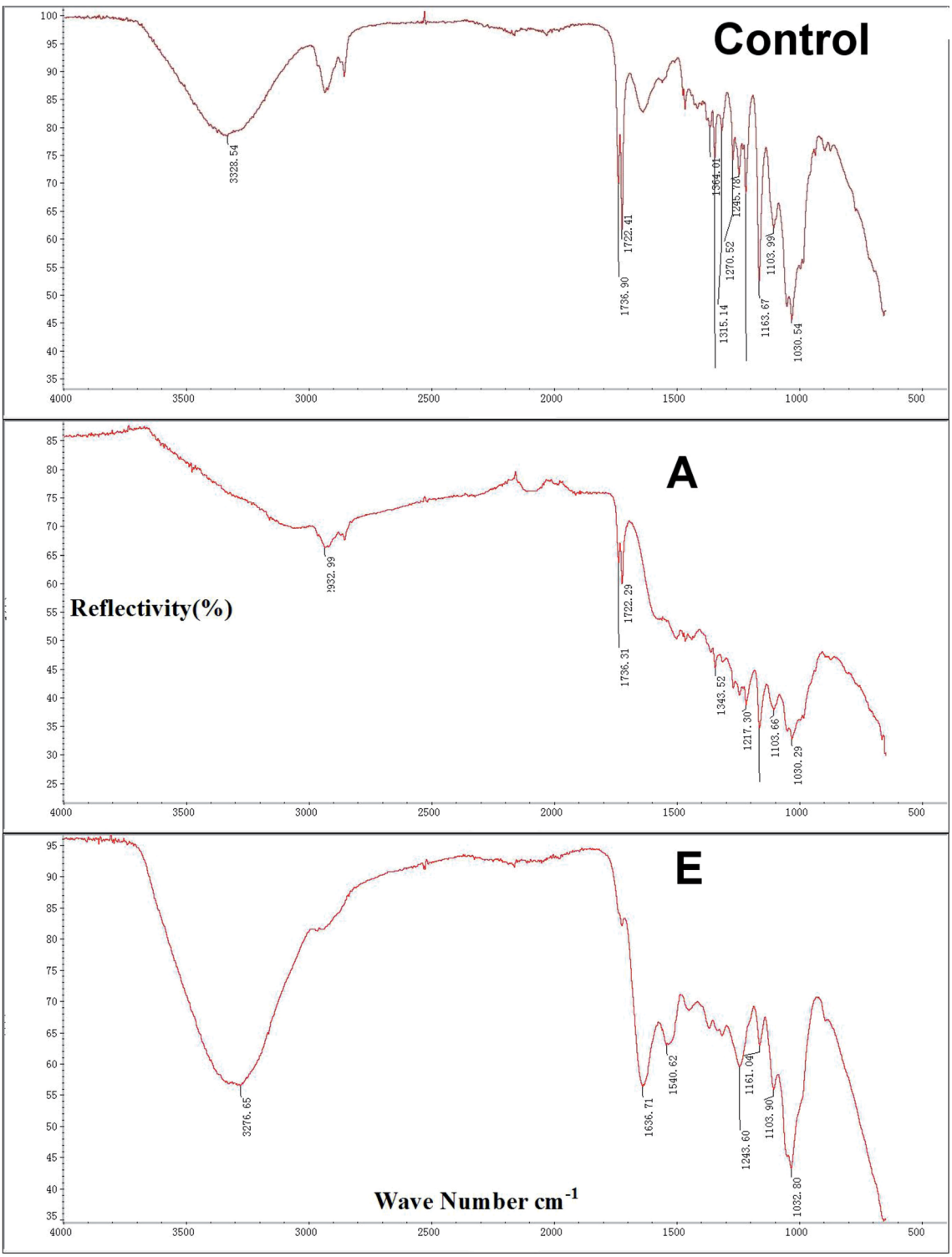

Fig. 3 The infrared spectra of the Control (delignified balsa), A (+dopamine), and E (20 mg ml^{-1} lysozyme) groups. And the *x*-coordinate was wave number cm^{-1}, the *y*-coordinate was reflectivity (%).

hydrogen bonds in the dopamine molecules. After surface modification, the peak shifted to near 1636.71 cm^{-1} because of the introduction of C=O structure. For D, the lysozyme showed two distinct characteristic peaks, corresponding to C=O stretching vibrations of amide I (1636.71 cm^{-1}) and N–H, flexural vibrations and C–N stretching vibrations of amide II (1032 cm^{-1}).

3.3 Contact angle test

As shown in Fig. 4, the average contact angle (θ) of the control group was 3.90 ± 0.85°, A was 4.61 ± 1.17°, and E was 19.46 ± 4.21°. Compared with group A and E, the difference was statistically significant ($P < 0.05$).

3.4 Enzyme loading and encapsulation efficiency and release *in vitro*

As shown in Fig. 5, with increased lysozyme concentration, the drug-loading rate of wood-lysozyme increased gradually, and the encapsulation efficiency decreased gradually ($P < 0.05$). The encapsulation efficiency of lysozyme at different concentrations was about 60%. The release rate of B, C, D and E groups tended to be stable and maximum at 48 h, with cumulative release percentages of 80.7%, 90.6%, 91.4% and 92.3% after 72 h.

3.5 Assay of antibacterial activity and test of cytotoxicity

As shown in Fig. 6, the growth of *S. aureus* and *E. coli* in the control group was in accordance with the normal trend. When

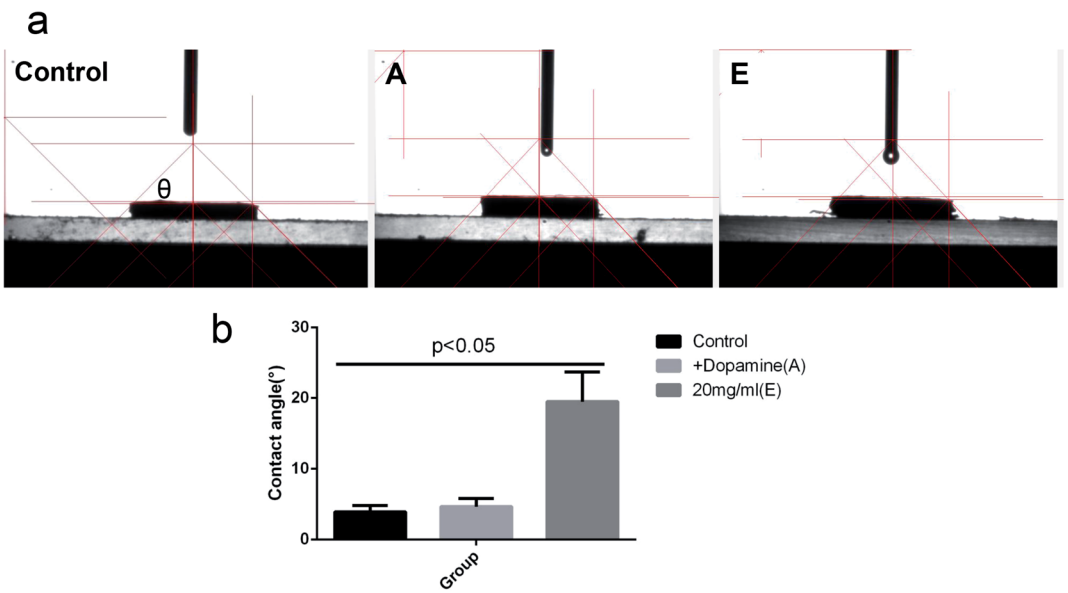

Fig. 4 (a): The contact angle (θ) of group control (delignified balsa), A (+dopamine), and E (20 mg ml^{-1} lysozyme). CA represents the contact angle value. (b): The statistics of contact angle.

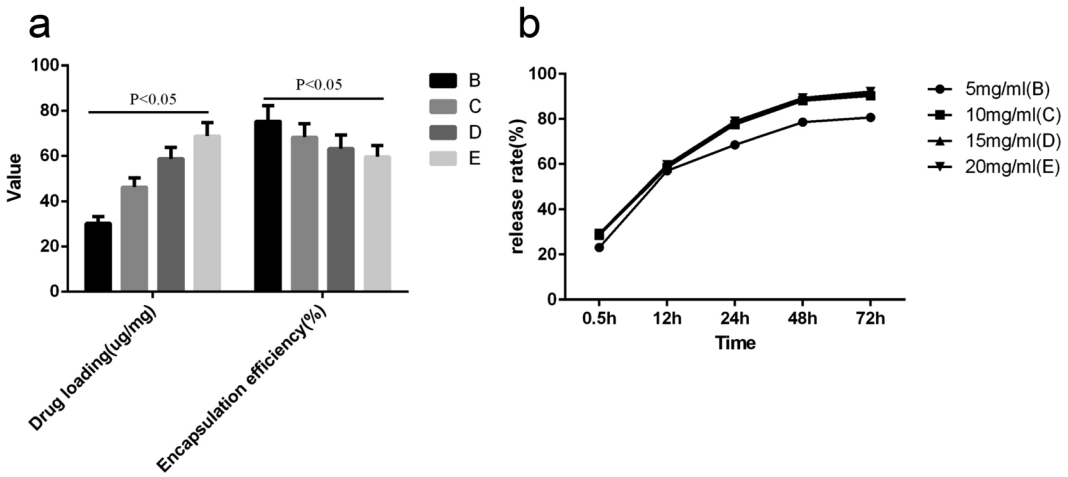

Fig. 5 (a) is the drug loading (μg mg^{-1}) and encapsulation efficiency of (%) of B (5 mg ml^{-1} lysozyme), C (10 mg ml^{-1} lysozyme), D (15 mg ml^{-1} lysozyme), E (20 mg ml^{-1} lysozyme) group. (b) is the drug release rate (%) of B, C, D, E group *in vitro*.

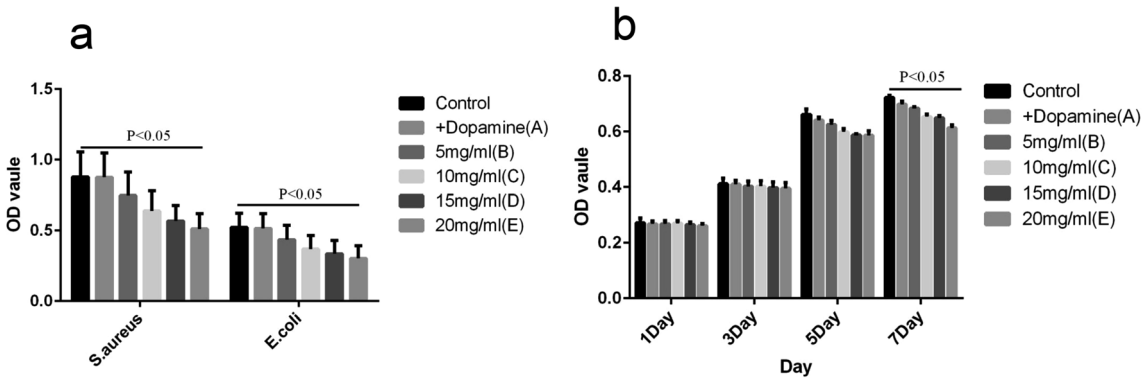

Fig. 6 Assay of antibacterial activity. (a) The OD value of each Control in 24 h. (b) Different strains of each group at different time points of specific antimicrobial OD.

the concentration of lysozyme increased gradually, the inhibitory effect on the bacteria gradually increased, and the difference was statistically significant ($P < 0.05$). Lysozyme at different concentrations showed little inhibition of cell growth ($P > 0.05$). Only on day 7, group E showed a slight inhibitory effect ($P < 0.05$).

3.6 Effect on infectious wound healing

As shown in Fig. 7, the average healing rates on day 3 were 17.9%, 20.6%, 25.8%, 30.1%, 30.9% and 31.5%, respectively for the control, A, B, C, D and E groups. The rates on day 7 were 30.7%, 38.3%, 50.7%, 61.2%, 61.9% and 62.4%, respectively. The average healing get completely healing were 14.7 day, 13.2 day, 11.9 day, 10.5 day, 10.1 day and 9.8 day, respectively for the Control, A, B, C, D and E groups. The wound healing rates were higher in the C, D and E groups than in other three groups ($P < 0.05$). The difference between the C, D and E groups was not significant ($P > 0.05$).

3.7 New epithelial length

As shown in Fig. 8, there was no significant difference in the length of new epithelium among the Control, A, and B groups on day 3 after injury ($P > 0.05$). The wound lengths on day 7 were 631.7 μm, 702.5 μm, 759.4 μm, 825.3 μm, 831.7 μm and 836.6 μm in the Control, A, B, C, D and E groups, respectively. The length of new epithelium in groups C, D and E were significantly

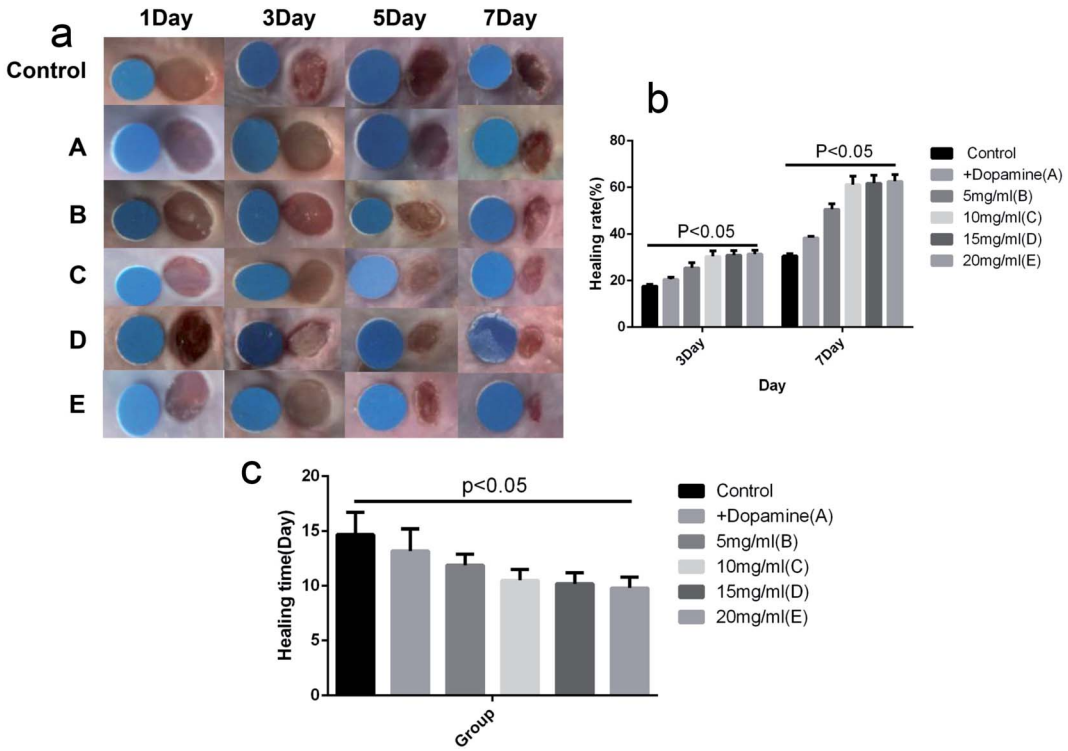

Fig. 7 Effect on infectious wound healing. (a) Wound healing map, the small round is the standard reference. (b) The wound healing statistics on 3, 7 day. (c) The time that wound required for complete healing.

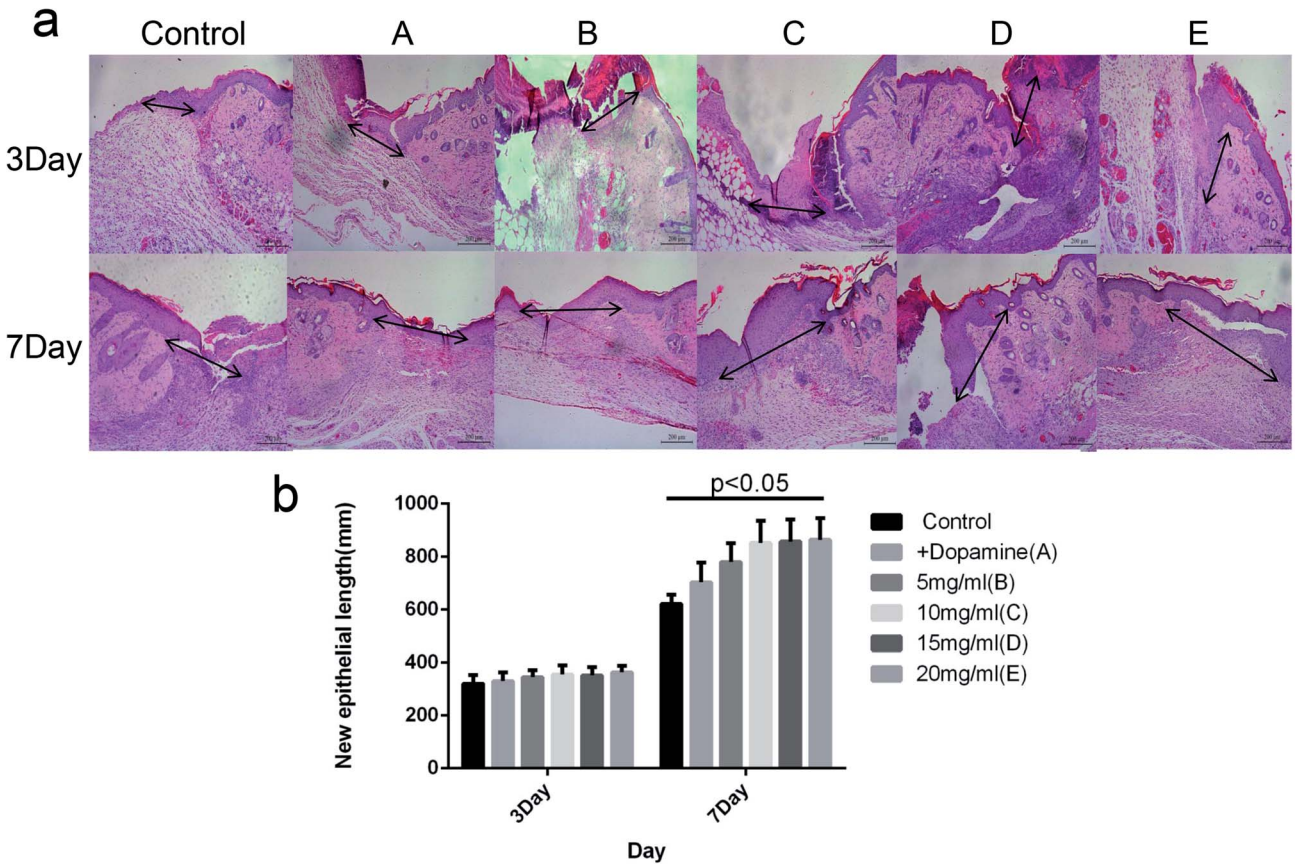

Fig. 8 HE staining of new epithelial length. (a) The length of the arrow represents the length of the new epithelial. (b) The statistics of length of the new epithelial.

higher than the other three groups ($P < 0.05$), and there was no significant difference between group C, D and E ($P > 0.05$).

3.8 Cell proliferation and angiogenesis

As shown in Fig. 9, the PCNA and CD31 expression levels were measured and the results indicated that cell proliferation and angiogenesis were enhanced when skin defects were covered with the C, D and E group ($P < 0.05$), which significantly accelerated wound healing. There was no significant difference between group C and E ($P > 0.05$).

4 Discussion

As shown in Fig. 2, the balsa retained the ordinary balsa structure (A1–3), and the texture was clear, consistent with previous studies.[5,20] The wood-lysozyme group showed some deposition under E1, E2, and E3, with visible dopamine layer and lysozyme (as crystals precipitated on the surface). We think that is because the lysozyme concentration of 20 mg ml^{-1} is much larger than that 2–5 mg ml^{-1} of other related research.[21,22] Lysozyme is composed of 129 amino acid residues, and the proportion of basic amino acid residues and aromatic amino acids and tryptophan residues is very high. Additionally, lysozyme contains four 2-disulfide bonds, consists of two regions connected by a long alpha helix, and has mostly alpha helical secondary structure.[9,10] As shown in Fig. 3, there are two typical two characteristic peaks of lysozyme,[11] but the intensity is decreased. This shows that the lysozyme molecule was immobilized on the carrier with a significant change in secondary structure. As shown in Fig. 4, both the Control and group A are mostly hydrophilic, indicating that the adhesion of dopamine did not change the characteristics of the material itself. Although E group was 19.46 ± 4.21°, it still has strong hydrophilicity, which can target the internal hydrophobicity of bacteria to allow lysozyme's antibacterial function.[7,8] As shown in Fig. 5, with increased lysozyme concentration, the drug loading rate of wood-lysozyme increased gradually and the encapsulation efficiency decreased gradually ($P < 0.05$). The higher the content of lysozyme, the more likely it is to be coated on the surface of balsa, which results in less content of lysozyme and low encapsulation efficiency.[7,9,10] However, the encapsulation efficiency of lysozyme at different concentrations was about 60%, suggesting this method was effective for lysozyme embedding. The release rates of B, C, D and E groups tended to be stable and highest at 48 h, with cumulative release percentages of 80.7%, 90.6%, 91.4% and 92.3% after 72 h. As for the release of drugs, lysozyme released faster in the first 24 h, suggesting early release may be possible. Because lysozyme is embedded in balsa structure by glue method.[8,11] The encapsulation structure is poor in density, and lysozyme has good water

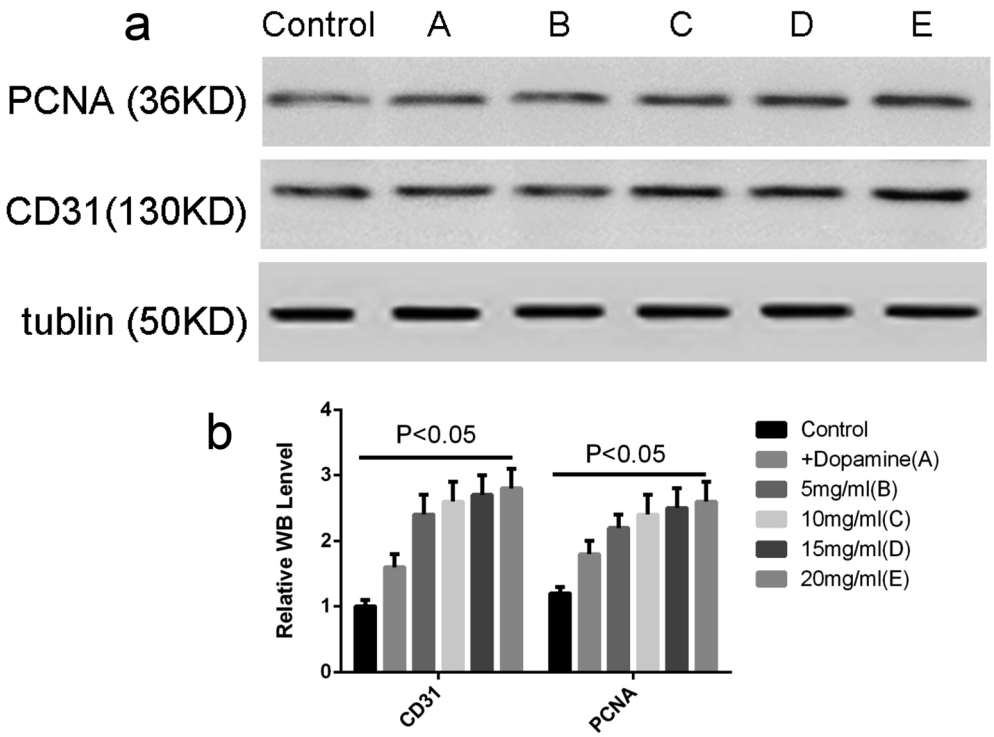

Fig. 9 Western blot to detect PCNA and CD31 expression. (a) The protein levels of PCNA and CD31 in the full-thickness wound tissues, as determined by western blot. (b) The OD values of the PCNA and CD31 bands in each group.

solubility. The lysozyme-balsa was cultured in PBS buffer solution and the lysozyme was easily released to PBS through the balsa surface structure, resulting in an increase in release.[21,22] After 48 h, the amount of lysozyme released from balsa remained almost unchanged, indicating that its release had stabilized and reached its maximum and fluctuated around 80–90%.

As shown in Fig. 6, the growth of *S. aureus* and *E. coli* in the control group was normal. When the concentration of lysozyme increased gradually, the inhibitory effect on the bacteria gradually increased, and the observed difference was statistically significant ($P < 0.05$). The lysozyme inhibits Gram-positive bacteria by hydrolysis of the 1,4-linkage between *N*-acetylmuramic acid and *N*-acetyl-D-glucosamine of bacterial cell peptidoglycan.[23] However, for Gram-negative bacteria, due to the protection of lipopolysaccharides, the sterilization effect is limited.[9] In recent years, there have been many studies to prepare lysozyme into microcapsules, nanoparticles, and pellets, and combine with different materials to improve its stability and its Gram-negative bacteria bactericidal effect.[7,10,11] Some studies have pointed out the hydrolysis activity of PTFE membrane loaded with lysozyme against the micrococcus lysate can reach 3.5 U cm^{-2}, which has perfect antibacterial activity against the important pathogenic *Staphylococcus aureus*, and the antibacterial rate reaches 89%. The antibacterial rate is expected to be further improved if the rate of enzyme load per unit area is increased.[15,18] In this study, the lysozyme was fully adhered to the pores by dopamine glue, providing a stable releasing microenvironment for Gram-negative bacteria. As shown in Fig. 8, only on day 7, group E showed a slight inhibitory effect ($P < 0.05$). Lysozyme is derived from egg white, and is generally considered a natural, safe enzyme, making it widely used for food preservation.[24]

When a burn occurs, the defense barrier on the body surface is destroyed, and the immune capacity is decreased. Extensive tissue necrosis and invasion of bacteria *in vivo* will lead to wound infection.[25] Wound infection is a major complication and key cause of death in burned patients. About 52–70% of burn patients die due to wound infection.[26] In this study, tested bacterial concentrations were 10^8 per ml^{-1}.[27–29] As shown in Fig. 7, the wound healing rates were higher in the C, D and E groups than in the other three groups ($P < 0.05$). The results suggest that the anti-infective effect increases and then plateaus (10 mg ml^{-1}). The wound healing process involves the contraction and the epithelization of the wound. For compact-skin species such as humans, wound healing is mainly driven by re-epithelialization.[30] There was no difference in the length of new epithelium in the groups after 3 days of injury ($p > 0.05$), mainly because the margins were still in the preparation period of cell proliferation and migration after 3 days of injury, so new epithelium was not obvious.[31] The results for wound length suggest that high concentrations of lysozyme might accelerate the healing of the wound by controlling infection and promoting re-epithelialization in the late post-injury period (7 days after injury, Fig. 8). The action mechanism of the lycid enzyme is the effect of rapid sterilization by the beta-1,4 glucoside bond in the cell wall peptidoglycan structure of the pathogen. In addition, the lysozyme also helps to enhance the

capacity of macrophages, improve the resistance of the human body and reduce the drug resistance.[28,31] Some studies suggest that lysostaphin can control the wound infection effectively, and use a large complex lysozyme concentration for 1–5 times to the wound can completely remove harmful microorganisms wound, its bactericidal ability to make people satisfied. However, there may be additional mechanisms to promote re-epithelialization. Angiogenesis is a related process that supports granulation tissue formation and provides the nutrition and oxygen necessary for tissue repair. The PCNA and CD31 expression indicated that cell proliferation and angiogenesis were enhanced when skin defects were covered with the C, D and E group ($P < 0.05$). There are limitations of this study. For example, improved dressing preparation, improved stability of lysozyme, and better efficacy against Gram negative bacilli are important goals of future work. Additionally, in future studies, we plan to design and study translucent wood-modified lysozyme.

5 Conclusion

This study prepared natural wood-lysozyme anti-infective dressings with different concentrations of lysozyme. Concentrations of 10–20 mg ml^{-1} were effective, and the wood-lysozyme dressing promoted wound healing. High concentration or long-term contact might inhibit cell proliferation. This dressing provides a new treatment for wound healing using natural materials.

Author contributions statement

All authors contributed to study design; ZD, MX and LG designed experiments; ZD and YT analyzed data and prepared tables and figures; and ZD wrote the manuscript.

Conflicts of interest

The authors declare no competing financial interests.

References

1 O. Vay, K. D. Borst, C. Hansmann, A. Teischinger and U. Müller, *Wood Sci. Technol.*, 2015, **49**, 577–589.
2 S. Trey, S. Jafarzadeh and M. Johansson, *Int. Mater. Rev.*, 2015, **60**, 431–450.
3 P. Nejat, F. Jomehzadeh, M. M. Taheri, M. Gohari and M. Z. A. Majid, *Renewable Sustainable Energy Rev.*, 2015, **43**, 843–862.
4 S. Wang, A. Lu and L. Zhang, *Prog. Polym. Sci.*, 2016, **53**, 169–206.
5 Y. Li, Q. Fu, S. Yu and M. Yan, *Biomacromolecules*, 2016, **17**, 1358–1364.
6 J. Jiang, C. Zhang, G. M. Zeng, J. L. Gong and Y. N. Chang, *J. Hazard. Mater.*, 2016, **317**, 416–429.
7 M. Jing, W. Song and R. Liu, *Spectrochim. Acta, Part A*, 2016, **164**, 103–109.
8 L. Zheng, Y. Wan, L. Yu and D. Zhang, *Talanta*, 2016, **146**, 299.
9 T. Zhang, P. Zhou, Y. Zhan, X. Shi, J. Lin, Y. Du, X. Li and H. Deng, *Carbohydr. Polym.*, 2015, **117**, 687–693.
10 C. B. Amara, N. Eghbal, P. Degraeve and A. Gharsallaoui, *J. Food Eng.*, 2016, **183**, 50–57.
11 S. Dekina, I. Romanovska, A. Ovsepyan, V. Tkach and E. Muratov, *Carbohydr. Polym.*, 2016, **147**, 208–215.
12 J. Jiang, C. Zhang, G. M. Zeng, J. L. Gong, Y. N. Chang, B. Song, C. Deng and H. Liu, *J. Hazard. Mater.*, 2016, **317**, 416–429.
13 M. Jing, W. Song and R. Liu, *Spectrochim. Acta, Part A*, 2016, **164**, 103–109.
14 S. Guo and L. A. Dipietro, *J. Dent. Res.*, 2010, **89**, 219–229.
15 R. Morsy, M. Hosny, F. Reicha and T. Elnimr, *Fibers Polym.*, 2016, **42**, 578–582.
16 L. W. Chan, C. H. Kim, X. Wang, S. H. Pun, N. J. White and T. H. Kim, *Acta Biomater.*, 2016, **31**, 178–185.
17 M. B. Dreifke, A. A. Jayasuriya and A. C. Jayasuriya, *Mater. Sci. Eng., C*, 2015, **48**, 651–662.
18 Y. Wang, R. Xu, G. Luo, Q. Lei, Q. Shu, Z. Yao, H. Li, J. Zhou, J. Tan, S. Yang, R. Zhan, W. He and J. Wu, *Acta Biomater.*, 2016, **30**, 246–257.
19 E. Cabane, T. Keplinger, T. Künniger, V. Merk and I. Burgert, *Sci. Rep.*, 2016, **6**, 31287.
20 M. Zhu, J. Song, T. Li, A. Gong and Y. Wang, *Adv. Mater.*, 2016, **28**, 5181–5187.
21 V. Grumezescu, A. M. Holban, L. E. Sima, M. B. Chiritoiu, G. N. Chiritoiu and A. M. Grumezescu, *Int. J. Pharm.*, 2017, **521**, 184–195.
22 L. Lin, H. Sun, K. Zhang, Y. Zhong and Q. Cheng, *J. Hazard. Mater.*, 2017, **327**, 97–107.
23 S. Yuan, J. Yin, W. Jiang, B. Liang, S. O. Pehkonen and C. Choong, *Colloids Surf., B*, 2013, **106C**, 11–21.
24 B. K. Tiwari, V. P. Valdramidis, C. P. O'Donnell, K. Muthukumarappan and P. Bourke, *J. Agric. Food Chem.*, 2009, **57**, 5987–6000.
25 F. Atsuki, S. Tamaki, F. Ken, K. Naoki, N. Teruo, T. Emi and U. Hisayuki, *Burns*, 2015, **41**, 956–968.
26 K. Ito, A. Saito, T. Fujie, K. Nishiwaki, H. Miyazaki, M. Kinoshita, D. Saitoh, S. Ohtsubo and S. Takeoka, *Acta Biomater.*, 2015, **24**, 87–95.
27 D. Costley, H. Nesbitt, N. Ternan, J. Dooley and Y. Y. Huang, *Int. J. Antimicrob. Agents*, 2017, **9**, 31–36.
28 W. A. Sarhan, H. M. E. Azzazy and I. M. Elsherbiny, *ACS Appl. Mater. Interfaces*, 2016, **8**, 6379–6390.
29 P. Chadha, O. P. Katare and S. Chhibber, *Microb. Pathog.*, 2016, **99**, 68–77.
30 N. Jangpromma, S. Preecharram, T. Srilert, S. Maijaroen, P. Mahakunakorn, N. Nualkaew, S. Daduang and S. Klaynongsruang, *J. Microbiol. Biotechnol.*, 2016, **26**, 1140–1147.
31 D. Liang, Z. Lu, H. Yang, J. Gao and R. Chen, *ACS Appl. Mater. Interfaces*, 2016, **8**, 3958–3968.

